Low-resistance ohmic contacts on InAlN/GaN heterostructures with MOCVD-regrown n$^+$-InGaN and mask-free regrowth process

Jingshu Guo(郭静姝)[1,2], Jiejie Zhu(祝杰杰)[1,2,†], Siyu Liu(刘思雨)[1,2], Jielong Liu(刘捷龙)[2,3], Jiahao Xu(徐佳豪)[1,2], Weiwei Chen(陈伟伟)[4], Yuwei Zhou(周雨威)[2,3], Xu Zhao(赵旭)[2,3], Minhan Mi(宓珉瀚)[1,2], Mei Yang(杨眉)[2,3], Xiaohua Ma(马晓华)[1,2,‡], and Yue Hao(郝跃)[1,2]

[1] *School of Microelectronics, Xidian University, Xi'an* 710071, *China*
[2] *The National Key Discipline Laboratory of Wide Bandgap Semiconductor, Xidian University, Xi'an* 710071, *China*
[3] *School of Advanced Materials and Nanotechnology, Xidian University, Xi'an* 710071, *China*
[4] *China Academy of Space Technology (Xi'an), Xi'an* 710100, *China*

(Received 24 April 2022; revised manuscript received 25 July 2022; accepted manuscript online 12 August 2022)

This paper studied the low-resistance ohmic contacts on InAlN/GaN with metal–organic chemical vapor deposition (MOCVD) regrowth technique. The 150-nm regrown n$^+$-InGaN exhibits a low sheet resistance of 31 Ω/□, resulting in an extremely low contact resistance of 0.102 Ω·mm between n$^+$-InGaN and InAlN/GaN channels. Mask-free regrowth process was also used to significantly improve the sheet resistance of InAlN/GaN with MOCVD regrown ohmic contacts. Then, the diffusion mechanism between n$^+$-InGaN and InAlN during regrowth process was investigated with electrical and structural characterizations, which could benefit the further process optimization.

Keywords: InAlN/GaN, low-resistance ohmic contacts, metal–organic chemical vapor deposition (MOCVD), n$^+$-InGaN, time of flight secondary ion mass spectrometry (TOF-SIMS)

PACS: 73.40.Cg, 73.40.Kp, 73.61.Ey **DOI:** 10.1088/1674-1056/ac891b

1. Introduction

GaN-based heterostructures with high-Al and thin barrier are desirable for the scale-down high-electron-mobility transistors (HEMTs), among which lattice-matched InAlN/GaN has attracted much attention for scale-down high frequency and low-voltage high efficiency applications.[1–5] However, low-resistance ohmic contact on high-Al-barrier heterostructures becomes a challenge.[6] This can cause high-frequency parasitic effects and drop of efficiency, which will be even much more serious for scale-down devices. In addition, the traditional alloy ohmic contact method usually results in the rough morphology and spikes, which will prevent the device from lateral scaling.[7–10] Therefore, excellent ohmic contact with low contact resistance and smooth surface morphology is of vital importance for InAlN/GaN HEMTs.

There have been various methods developed to achieve low ohmic contact in GaN-based devices, such as recess-arrayed ohmic contacts, Si/Ge pre-deposition, ion implantation, regrown heavily-doped GaN, *et al.*[11–14] For ultra-scale deices, regrown ohmic contact method has its superiority in extremely low contact resistance and smooth surface. In order to achieve selective epitaxy of highly doped n$^+$-GaN in the ohmic region, a layer of SiO_2 is usually grown on the surface of the heterojunction by plasma enhanced chemical vapor deposition (PECVD) as a hard mask, and it is removed by wet corrosion process after epitaxy is completed. Regrowth of n$^+$-GaN by molecular beam epitaxy (MBE) has resulted in ohmic contact resistance as low as ∼ 0.1 Ω·mm in various GaN-based heterostructures including InAlN/GaN, AlGaN/GaN, AlN/GaN, and so on.[15–17] Low contact resistance of 0.16 Ω·mm in AlGaN/GaN structure has also been achieved with heavily doped material regrown by metal–organic chemical vapor deposition (MOCVD), which has the advantages of production capacity and cost.[18–20] However, few reports have involved in the regrown ohmic contacts of InAlN/GaN using MOCVD, because the high temperature regrowth process will cause another challenge on the degradation of InAlN.

In this paper, we demonstrated the low resistance ohmic contacts on the InAlN/GaN heterostructure with MOCVD regrowth technique. The n$^+$-InGaN regrowth material instead of traditional n$^+$-GaN was adopted, which helped to significantly reduce the heat budget during the regrowth process. In addition, mask-free regrowth process was developed in this work to avoid the serious influence of commonly used SiO_2 mask on InAlN/GaN degradation during high-temperature regrowth process. Extremely low contact resistance between n$^+$-InGaN and InAlN/GaN channels of 0.102 Ω·mm was achieved, with a moderate two-dimensional (2D) electron gas (2DEG) sheet resistance of 397 Ω/□. Finally, capacitance–voltage (C–V) and time of flight secondary ion mass spectrometry (TOF-SIMS) analysis was used to further investigate the influence mechanism of the n$^+$-InGaN regrowth process on the InAlN/GaN channel.

†Corresponding author. E-mail: jjzhu@mail.xidian.edu.cn
‡Corresponding author. E-mail: xhma@xidian.edu.cn

© 2023 Chinese Physical Society and IOP Publishing Ltd

2. Devices fabrication

InAlN/GaN epitaxial layers used in this work were grown by MOCVD, consisting of GaN buffer, 300-nm unintentionally doped GaN channel layer, 1-nm AlN interlayer, and 2-nm GaN cap layer on 8-nm $In_{0.17}Al_{0.83}N$ barrier layer. The Hall measurement at room temperature shows a sheet carrier density of 2.29×10^{13} cm^{-2}, mobility of 1323 cm^2/V·s, and a sheet resistance of 207 Ω/□. The process flow of MOCVD regrown-ohmic contacts was shown in Fig. 1. At the beginning of the ohmic regrowth process, the unintentionally doped InAlN and GaN in the ohmic region were removed by photolithography and dry etching. In order to ensure the contact between n$^+$-InGaN and 2DEG in the channel, the etching depth is greater than 30 nm. Wet treatment with ammonia had been carried out to remove the Cl contaminant and native oxide from the GaN surface.[21,22] And 150-nm-thick n$^+$-InGaN which contains 5% In was grown by MOCVD at 800 °C with Si doping concentration of 10^{20} cm^{-3}. Then, Ti/Au electrodes were prepared over n$^+$-InGaN in the source/drain region by electron beam evaporation. After that, the n$^+$-InGaN covering the barrier was removed by self-terminating etching.[23] Finally, device mesa isolation was performed by dry etching.

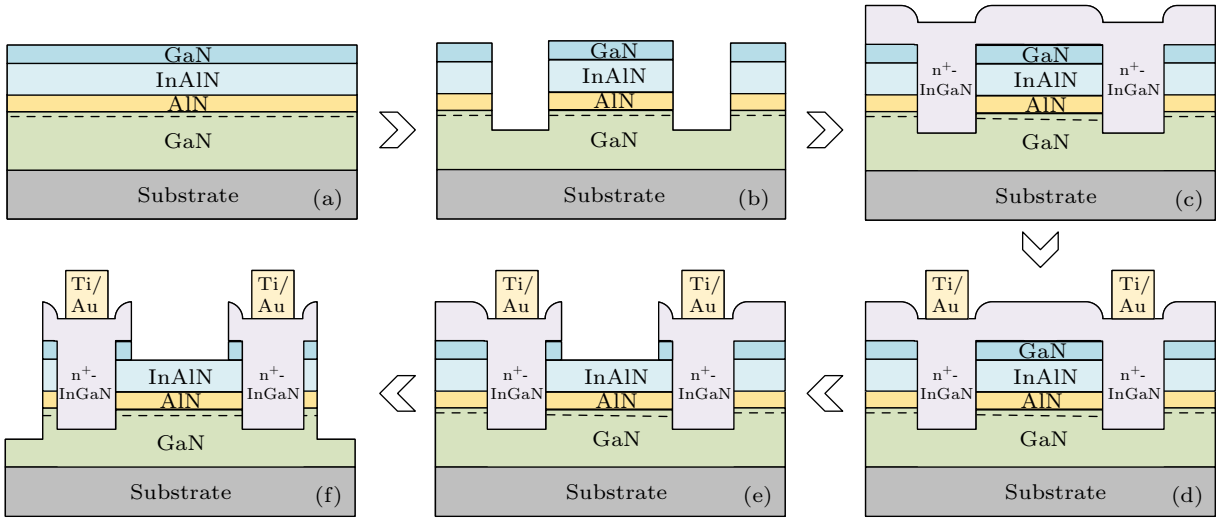


Fig. 1. The process flow of mask-free MOCVD regrown-ohmic contacts on InAlN/GaN.

3. Results and discussion

To study the surface coverage of the ohmic contact and the crystalline quality of n$^+$-InGaN, the sample with n$^+$-InGaN were observed by transmission electron microscopy (TEM). As shown in Fig. 2, region 1 and region 2 were enlarged and shown in Figs. 2(b) and 2(c), respectively. It can be seen in Fig. 2(b) that the n$^+$-InGaN grown by MOCVD has high crystallinity. At the ohmic contact edge, the etching inclination angle is greater than 70°, which means that the etching is highly anisotropic.[24,25] Such a steep sidewall can reduce the depletion of 2DEG at the etched edge. Moreover, the edge of the step is well covered, which is necessary to form excellent ohmic contact. From the profile of InAlN/GaN heterojunction in Fig. 2(c), it is interesting that both InAlN barrier and GaN channel after the MOCVD regrowth have high crystalline quality. No significant precipitation of In was observed.

The contact resistance and material resistivity were extracted by transmission line models (TLM).[26] The results for the InAlN/GaN with MOCVD regrown n$^+$-InGaN were shown in Table 1. The schematics for the ohmic contacts were shown in Fig. 3(a). The resistance for regrowing ohmic contact consists of three parts. The contact resistance between Ti/Au electrode and n$^+$-InGaN (R_{m_n}) is 0.046 Ω·mm. And the resistance of the 1.5-μm n$^+$-InGaN from metal to the 2DEG edges (R_n) is as low as 0.047 Ω·mm, which is mainly due to the low resistivity of 31 Ω/□ of n$^+$-InGaN. Based on the above values and the total resistance of 0.195 Ω·mm, the contact resistance between n$^+$-InGaN and GaN channels (R_{n_ch}) is calculated to be 0.102 Ω·mm, which is also the best value of the MOCVD ohmic regrowth on InAlN/GaN. The R_{sh} of 397 Ω/□ is an excellent value in InAlN/GaN with MOCVD regrown ohmic contacts. Compared with n$^+$-GaN, n$^+$-InGaN can achieve lower resistivity with higher Si-doping concentration at lower growth temperature. And this effectively weaken the influence of MOCVD on the InAlN barrier.[27,28] In addition, the mask-free regrowth process avoids the serious influence of SiO_2 mask on InAlN/GaN during high-temperature regrowth process. To give a more accurate assessment of the process, the sample was compared with devices that achieve ohmic contact by alloying. The on resistance (R_{on}) with respect to different source-drain spacing (L_{sd}) was shown in Fig. 3(b). When the L_{sd} is greater than 5 μm, the R_{on} of devices with alloyed ohmic contacts is smaller, but when L_{sd} is less than 4 μm, the MOCVD regrowth process is more advantageous. And this shows a very significant advantage in the application of millimeter wave devices. In addition, the 2DEG surface density of the device that achieves ohmic contact through n$^+$-InGaN was

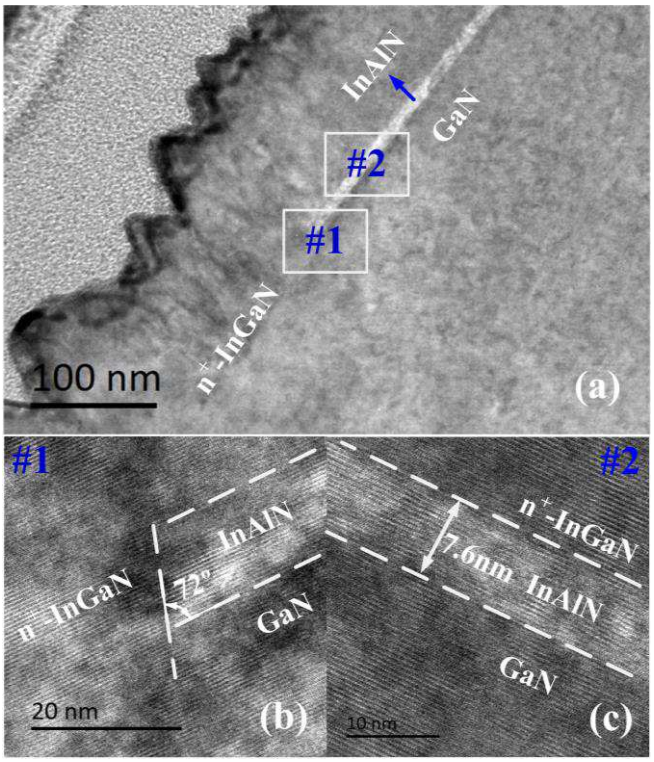


Fig. 2. (a) TEM picture and (b), (c) the partially enlarged view of InAlN/GaN with MOCVD regrown n$^+$-InGaN ohmic contacts.

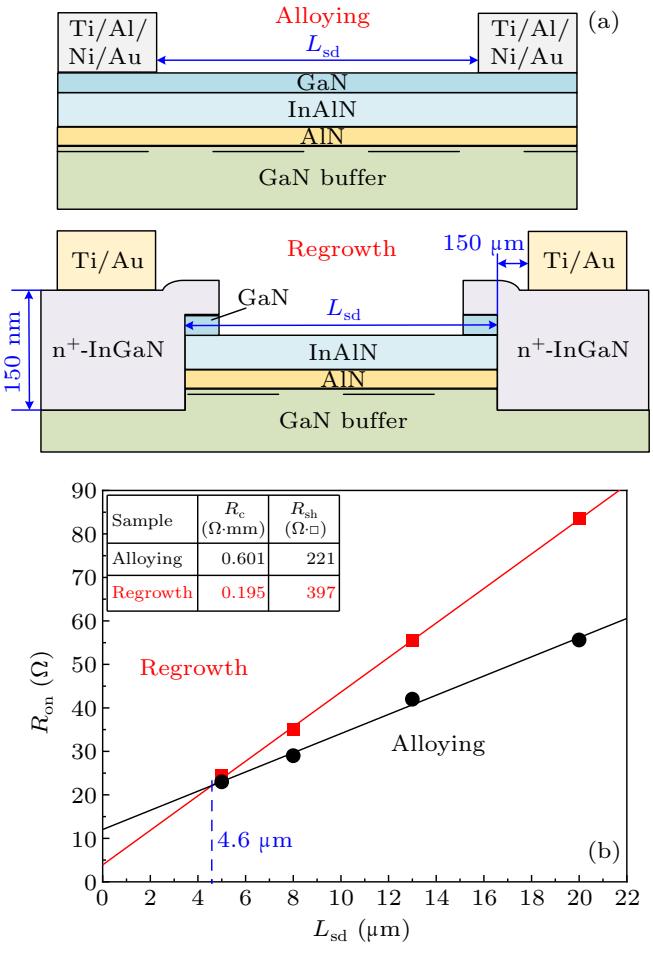


Fig. 3. (a) Schematics and (b) the on resistance (R_{on}) *versus* source–drain spacing (L_{sd}) of sample with alloying ohmic contacts and with regrown ohmic contacts by MOCVD.

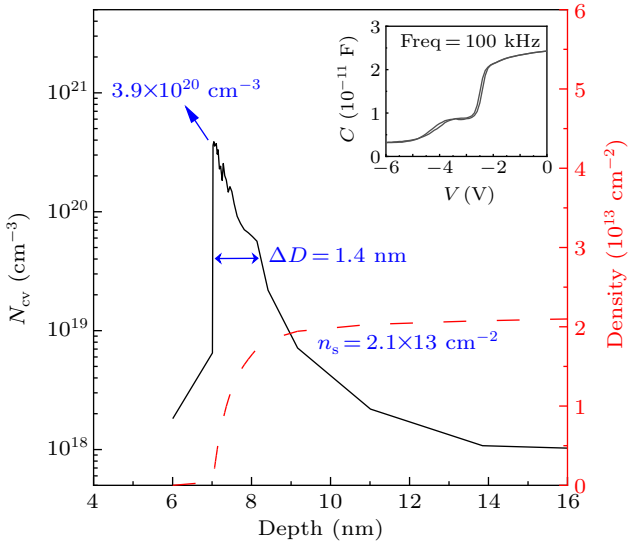


Fig. 4. . Carrier concentration distributions of the sample with n$^+$-InGaN grown by MOCVD.

Table 1. Contact and sheet resistance value.

Contact resistance (Ω·mm)	R_{m_n}	0.046
	R_n	0.047
	R_{n_ch}	0.102
Sheet resistance (Ω·mm)	n$^+$-InGaN	31
	2DEG	397

extracted through C–V test at 100 kHz, and the results were shown in Fig. 4. The carrier concentration (N_{cv}) was calculated from the slope dC/dV of the C–V curve which was illustrated. And from the space-charge region width, the depth can be obtained. The 2DEG density was calculated by integrating the N_{cv}–depth curve.[29,30] After the n$^+$-InGaN regrowth, the 2DEG surface density still as high as 2.1×10^{13} cm^{-2} with a peak concentration of 3.9×10^{20} cm^{-3}. There is a small step near the peak concentration, which may be related to the increase of R_{sh}.

According to the characteristics of the MOCVD processes, the In composition of InAlN maybe separate out at high temperature, which may lead to a significant increase of R_{sh}. In order to study this problem, detailed analysis on components of the n$^+$-InGaN and the InAlN/GaN was conducted by TOF-SIMS. The curves of ion count radio versus sputtering time in TOF-SIMS were shown in Fig. 5. In the GaN/InAlN/GaN sample shown in Fig. 5(a), the distribution of In, Ga, and Al have clear boundaries at the interface. The AlN spacer below the InAlN results in a higher Al component than that of the upper surface of InAlN. And it can enhance polarization effect and weaken the scattering effect.[31] However, because of the transition region between AlN layer and GaN layer of MOCVD epitaxy and the limited accuracy of SIMS analysis, it is difficult to accurately mark the position of 1-nm-thick AlN.[32] After the MOCVD regrowth, as shown in Fig. 5(b), the wide component gradient area in the n$^+$-InGaN/GaN/InAlN/GaN sample indicates that diffusion appears in InAlN/GaN and n$^+$-InGaN. However, the peak value

of In component did not decrease significantly. Moreover, the In and the Ga components of the n^+-InGaN shown in Fig. 5(c) are very evenly distributed. In addition to surface contamination, the distribution of doped Si in the n^+-InGaN layer is also consistent. And there is almost no Al component in the n^+-InGaN, except for a small amount of aluminum near the InAlN barrier layer, which is mainly related to the diffusion of Al in the barrier. It can also be seen from Fig. 5(b) that this part of Al diffusing from the barrier to n^+-InGaN is a very small amount. According to the above analyses, the diffusion processes can be divided into two types. One is internal diffusion at the interface, and the other is non-restricted surface source diffusion at the upper surface. The internal diffusion mainly related to the temperature and the time of MOCVD epitaxial process, which conforms to gaussian distribution. The non-restricted surface source diffusion can be described by the following residual error distribution function,[33]

$$N(x,t) = N_s \mathrm{erfc}\left(-\frac{x}{2\sqrt{Dt}}\right), \tag{1}$$

where N_s is the constant surface diffusion source concentration, x is the distance from the surface, D is the diffusion coefficient, and t is the diffusion time. The diffusion mechanism of Al component is mainly internal diffusion. The distribution of Ga and In is affected by the two diffusion mechanisms, of which the non-restricted surface source diffusion is the most significant. By comparing the distribution of In and Ga, it can be found that the surface source diffusion of Ga has a stronger effect. Because the Ga–N bond is stronger than the In–N bond, and Ga is more easily incorporated into the lattice.[34] And these eventually lead to the heterojunction with a gradient component barrier after MOCVD regrowth. Moreover, the two diffusion effects of Ga lead to the composition change of AlN spacer. It can be known from the residual error distribution equation that the diffusion concentration is directly related to the distance from the surface and the diffusion coefficient. In addition to reducing the temperature, covering the barrier with a suitable diffusion barrier can not only increase the distance from the InAlN barrier to the surface but also reduce the diffusion coefficient, which will obviously improve the process.

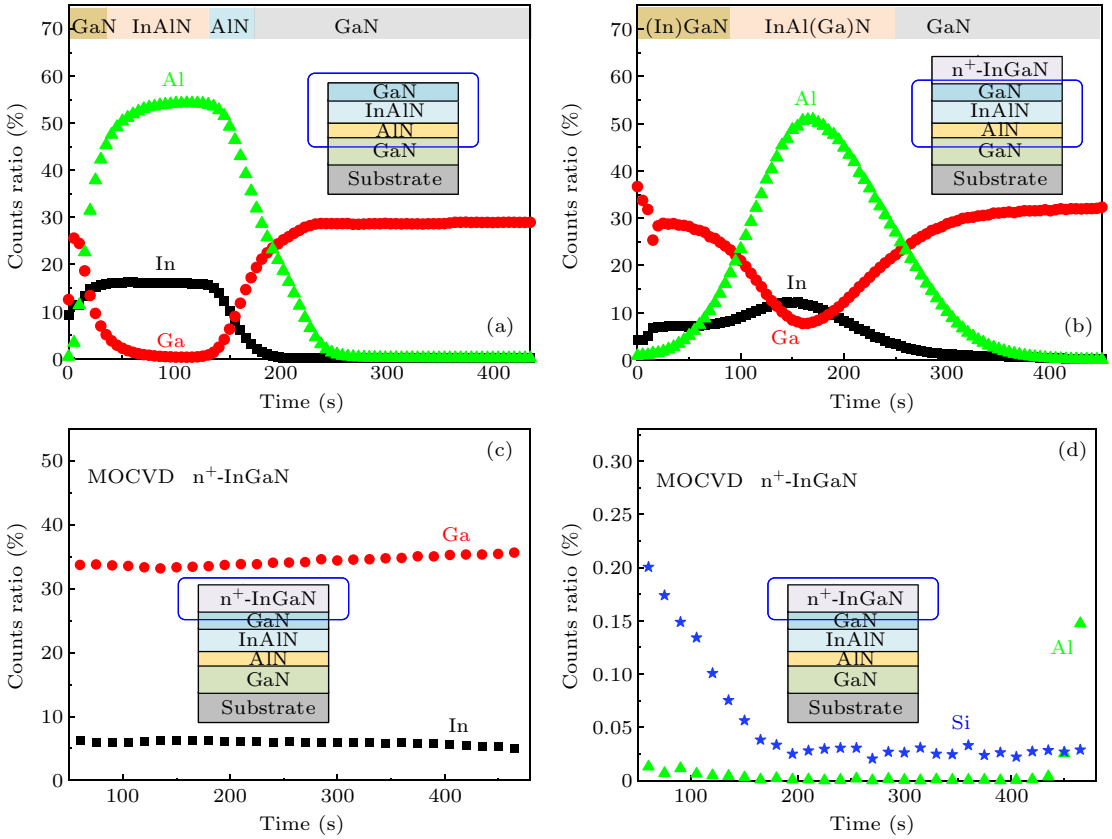


Fig. 5. The compositional analysis of InAlN/GaN in (a) GaN/InAlN/GaN and (b) n^+-InGaN/GaN/InAlN/GaN by TOF-SIMS. (c) Ga, In (d) Si and Al in the n^+-InGaN grown by MOCVD.

With the change of components in the heterojunction, the energy band changes. The conduction band of the barrier layer near the interface with a wide gap decreases, while that of the GaN channel with a narrow gap increases.[35,36] For the gradient structure, the electron affinity (χ) near the interface changes continuously with the coordinate x, which can be described by the following diffusion law distribution model:

$$\chi(x) = \left(\frac{\Delta\chi}{2}\right)\tanh\left(\frac{x}{L}\right), \tag{2}$$

where $\Delta\chi$ is the total variation of electron affinity in the two materials, and L is the width of the gradient region. As shown

in Fig. 6(a), before epitaxy of n^+-InGaN, the InAlN/GaN heterojunction shows a deep potential well and a high barrier height. The 2DEG in the channel has strong quantum confinement. After the regrowth of n^+-InGaN, the wider gradient region results in a shallower potential well. The diffusion of Ga leads to a narrowing of the bandgap in the AlN spacer and a significant decrease in the barrier height. The weakened quantum confinement on electrons and the enhanced scattering effect results in the larger sheet resistance.

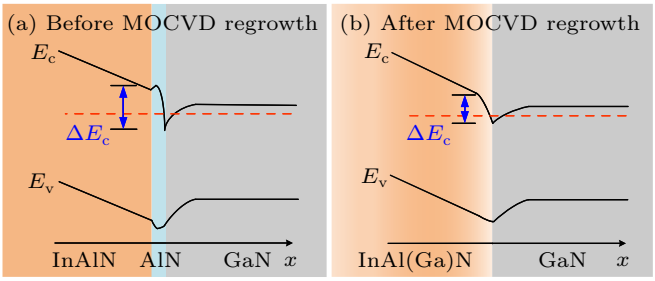


Fig. 6. Energy band of InAl(Ga)N/GaN (a) before and (b) after n^+-InGaN regrowth.

4. Conclusion

In conclusion, highly Si-doped n^+-InGaN with an ultra-low resistivity of 31 Ω/□ was grown by MOCVD. By the SiO_2-free ohmic regrowth technology, a low contact resistance of 0.102 Ω·mm between n^+-InGaN and InAlN/GaN channels was realized on InAlN/GaN with a much improving 2DEG R_{sh} of 397 Ω/□. And this technology has shown significant advantages in the application of millimeter wave devices with L_{sd} less than 4 μm. To provide a theoretical basis for further optimization of the process, the causes of the increasing R_{sh} in terms of the electrical characteristics and material structural were analyzed in detail. It was found that the non-restricted surface source diffusion plays a more important role in increasing the R_{sh} of the InAlN/GaN, which can be suppressed by covering the InAlN with a diffusion barrier.

Acknowledgments

Project supported by the Fundamental Research Funds for the National Key Research and Development Project of China (Grant No. 2020YFB1807403), the National Natural Science Foundation of China (Grant Nos. 62174125 and 62131014), the Fundamental Research Funds for the Central Universities (Grant Nos. QTZX22022 and YJS2213), and the Innovation Fund of Xidian University.

References

[1] Kuzmík J 2001 *IEEE Electron Dev. Lett.* **22** 510
[2] Then H W, Chow L A, Dasgupta S, Gardner S, Radosavljevic M, Rao V R, Sung S H, Yang G and Chau R S 2015 *Symposium on VLSI Technology*, June 16–18, 2015, Kyoto, Japan pp. T202–T203
[3] Wang R, Li G, Laboutin O, Cao Y, Johnson W, Snider G, Fay P, Jena D and Xing H 2011 *IEEE Electron Dev. Lett.* **32** 892
[4] Mi M, Wu S, Zhang M, Yang L, Hou B, Zhao Z, Guo L, Zheng X, Ma X and Hao Y 2019 *Appl. Phys. Express* **12** 114001
[5] Mi M, Zhang M, Wu S, Yang L, Hou B, Zhou Y, Guo L, Ma X and Hao Y 2020 *Chin. Phys. B* **29** 057307
[6] Abid I, Mehta J, Cordier Y, Derluyn J, Degroote S, Miyake H and Medjdoub F 2021 *Electronics* **10** 635
[7] Zhang L Q, Shi J S, Huang H F, Liu X Y, Zhao S X, Wang P F and Zhang D W 2015 *IEEE Electron Dev. Lett.* **36** 896
[8] Hou M, Xie G and Sheng K 2018 *IEEE Electron Dev. Lett.* **39** 1137
[9] Yadav Y K, Upadhyay B B, Meer M, Bhardwaj N, Ganguly S and Saha D 2019 *IEEE Electron Dev. Lett.* **40** 67
[10] Tsou C W, Kang H C, Lian Y W and Hsu S 2016 *IEEE Trans. Electron Dev.* **63** 4218
[11] Lu Y, Ma X, Yang L, Hou B, Mi M, Zhang M, Zheng J, Zhang H and Hao Y 2018 *IEEE Electron Dev. Lett.* **39** 1137
[12] Lin Y K, Noda S, Lo H C, Liu S C, Wu C H, Wong Y Y, Luc Q H, Chang P C, Hsu H T, Samukawa S and Chang E Y 2016 *IEEE Electron Dev. Lett.* **37** 1395
[13] Tzou A J, Hsieh D H, Chen S H, Li Z Y, Chang C Y and Kuo H C 2016 *Semicond. Sci. Technol.* **31** 055003
[14] Guo J, Cao Y, Lian C, Zimmermann T, Li G, Verma J, Gao X, Guo S, Saunier P, Wistey M, Jena D and Xing H G 2011 *Physica Status Solidi A* **208** 1617
[15] Li L, Nomoto K, Pan M, Li W, Hickman A, Miller J, Lee K, Hu Z, Bader S J, Lee S M, Hwang C M, Jena D and Xing H G 2020 *IEEE Electron Dev. Lett.* **41** 689
[16] Tang Y, Shinohara K, Regan D, Corrion A, Brown D, Wong J, Schmitz A, Fung H, Kim S and Micovic M 2015 *IEEE Electron Dev. Lett.* **36** 896
[17] Joglekar S, Azize M, Beeler M, Monroy E and Palacios T 2016 *Appl. Phys. Lett.* **109** 041602
[18] Guo H Y, Lv Y J, Gu G D, Dun S B, Fang Y L, Zhang Z R, Tan X, Song X B, Zhou X Y and Feng Z H 2015 *Chin. Phys. Lett.* **32** 118501
[19] Hatui N, Krishna A, Li H, Gupta C, Romanczyk B, Acker-James D, Ahmadi E, Keller S and Mishra U K 2020 *Semicond. Sci. Technol.* **35** 095002
[20] Koksaldi O S, Romanczyk B, Haller J, Guidry M, Li H, Keller S and Mishra U K 2020 *Semicond. Sci. Technol.* **35** 124004
[21] Dialea M, Aureta F D, Berga N G van der, Odendaala R Q and Roosb W D 2005 *Appl. Surf. Sci.* **246** 279
[22] Prabhakaran K, Andersson T G and Nozawa K 1996 *Appl. Phys. Lett.* **69** 3212
[23] Zhou Y, Mi M, Yang M, Han Y, Wang P, Chen Y, Liu J, Gong C, Lu Y, Zhang M, Zhu Q, Ma X and Hao Y 2022 *Appl. Phys. Lett.* **120** 062104
[24] Gary S M and Simon M S 2007 *Fundamentals of semiconductor fabrication* translated by Dai Y P (Peking: Posts and Telecom Press) p. 80 (in Chinese)
[25] Guo X H, Hu L, Ren X Y, Wu S, Zhang L Q, Zhang Z J, Yang H and Liu J P 2021 *Chinese Journal of Luminescence* **42** 889
[26] Guo J, Li G, Faria F, Cao Y, Wang R, Verma J, Gao X, Guo S, Beam E, Ketterson A, Schuette M, Saunier P, Wistey M, Jena D and Xing H 2012 *IEEE Electron Dev. Lett.* **33** 525
[27] Fu X C, Lv Y J, Zhang L J, Zhang T, Li X J, Song X B, Zhang Z R, Fang Y L and Feng Z H 2018 *Electron. Lett.* **54** 783
[28] Suzuki A, Choe S, Yamada Y, Otsuka N and Ueda D 2016 *Jpn. J. Appl. Phys.* **55** 121001
[29] Yang L, Zhang M, Hou B, Mi M, Wu M, Zhu Q, Lu Y, Zhu J, Zhou X, Lv L, Ma X and Hao Y 2020 *IEEE Trans. Electron Dev.* **67** 4808
[30] Zhu Q, Ma X, Hou B, Wu M, Zhu J, Yang L, Zhang M and Hao Y 2020 *IEEE Access* **8** 35520
[31] Pandey S, Cavalcoli D, Minj A, Fraboni B, Cavallini A, Gamarra P and Poisson M A 2012 *J. Appl. Phys.* **112** 123721
[32] Godejohann B J, Ture E, Muller S, Prescher M, Kirste L, Aidam R, Polyakov V, Bruckner P, Breuer S, Kohler K, Quay R and Ambacher O 2017 *Phys. Status Solidi B* **254** 1600715
[33] Katayama M 1991 *J. Appl. Phys.* **69** 3541
[34] Bedair S M, McIntosh F G, Roberts J C, Piner E L, Boutros K S and El-Masry N A 1997 *J. Cryst. Growth* **178** 32
[35] Wang J, Xu F, Zhang X, An W, Li X Z, Song J, Ge W, Tian G, Lu J, Wang X, Tang N, Yang Z, Li W, Wang W, Jin P, Chen Y and Shen B 2014 *Sci. Rep.* **4** 6521
[36] Dasgupta S, Nidhi, Brown D F, Wu F, Keller S, Speck J S and Mishra U K 2010 *Appl. Phys. Lett.* **96** 143504